

Performance of the MITC3+ and MITC4+ shell elements in widely-used benchmark problems

Yeongbin Ko ^a, Youngyu Lee ^b, Phill-Seung Lee ^{a,*}, Klaus-Jürgen Bathe ^c

^a Department of Mechanical Engineering, Korea Advanced Institute of Science and Technology, 291 Daehak-ro, Yuseong-gu, Daejeon 34141, Republic of Korea

^b Agency for Defense Development, Yuseong-gu, Daejeon 34186, Republic of Korea

^c Department of Mechanical Engineering, Massachusetts Institute of Technology, Cambridge, MA 02139, USA



ARTICLE INFO

Article history:

Received 17 June 2017

Accepted 4 August 2017

Keywords:

Shell structures
Shell finite elements
3- and 4-node elements
MITC method
Convergence study
Benchmark tests

ABSTRACT

Recently, new 3-node and 4-node MITC shell elements, the MITC3+ and MITC4+ elements, have been proposed. The two shell elements were tested through theoretically well-established convergence studies. In this paper we continue to investigate the performance of the MITC3+ and MITC4+ shell elements in relatively simple but widely adopted benchmark problems. To perform these tests as usually done, the predictive capability of the elements is assessed through point-wise convergence of displacements at specific locations of shell structures. The results obtained using the MITC3+ and MITC4+ shell elements are compared with those found for some other shell elements.

© 2017 Elsevier Ltd. All rights reserved.

1. Introduction

For the last several decades, the finite element method has been dominantly used for the analysis of shell structures. However, although a great effort has been expended since the 1950s to develop effective shell finite elements, “ideal” shell elements were not reached. The difficulty is due to the highly sensitive and complicated behavior of shell structures [1,2]. Ideal shell elements should satisfy the consistency, ellipticity and inf-sup conditions and show optimal solution convergence for all asymptotic categories of shell behaviors (membrane dominated, bending dominated and mixed behaviors) regardless of shell geometry, boundary and loading conditions, and mesh patterns used [1–8].

The main challenge to obtain such shell elements is to reduce and ideally eliminate “locking”. When a finite element discretization is deficient in approximating the displacement fields of shells, the solution accuracy deteriorates. This phenomenon is called “locking” and becomes more severe as the shell thickness decreases [1,2,9]. The MITC (Mixed Interpolation of Tensorial Components) method [1] has been effectively adopted for remedying shear and membrane locking present in shell finite elements. The 4-node MITC4 shell element has been widely used in engineering practice due to its simple formulation and excellent performance

[10]. Subsequently, a 3-node MITC3 shell element was proposed [11].

In further research, two new MITC shell elements (the MITC3+ and MITC4+ elements) were developed [3–5]. The MITC3+ shell element outperforms the MITC3 shell element and the MITC4+ shell element provides a significantly improved performance in distorted meshes compared to the MITC4 shell element [3–5]. Indeed, the behavior of these shell elements is very close to optimal. The elements, of course, pass all the basic tests; the zero energy mode, isotropy, and patch tests.

The MITC3+ and MITC4+ shell elements were tested through convergence studies in various membrane and bending dominated shell problems – in “all-encompassing test problems” – considering uniform and distorted meshes. The “all-encompassing” refers to the fact that membrane and bending dominated problems of shells with positive and negative Gaussian curvatures are included. The errors in the shell element solutions were measured using the s-norm [12], and the solution convergence rates with decreasing shell thickness were compared with the optimal convergence rates. This test procedure is theoretically well-founded but requires special coding for the calculation of the s-norm [1,12].

In previous research on shell elements this norm was not used and hence a comparison of the predictive capabilities of the MITC shell elements with published solution data requires that the previously used problems and solution measurements are employed. There exist some test problems of shell elements that have been

* Corresponding author.

E-mail address: phillseung@kaist.edu (P.S. Lee).

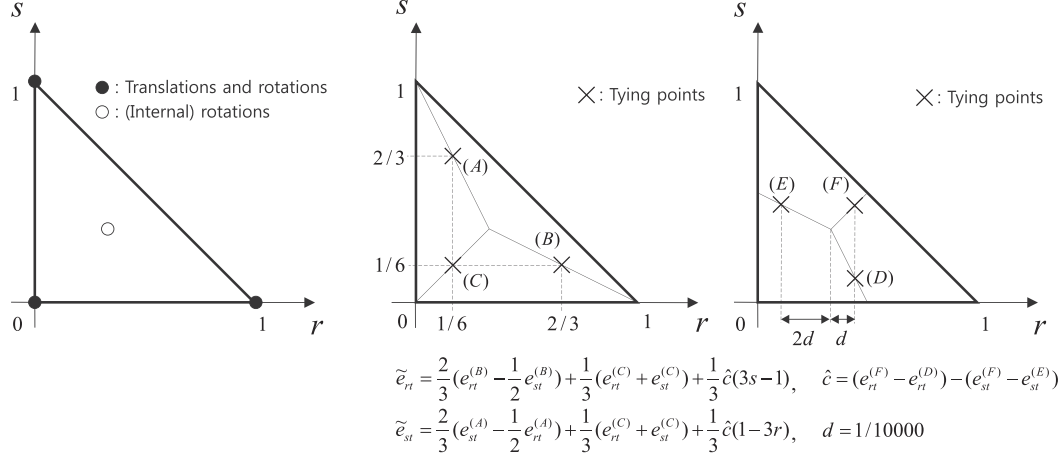


Fig. 1. The 3-node MITC3+ shell element. The coordinates r and s are in the two in-plane directions, and t is in the direction through the shell thickness.

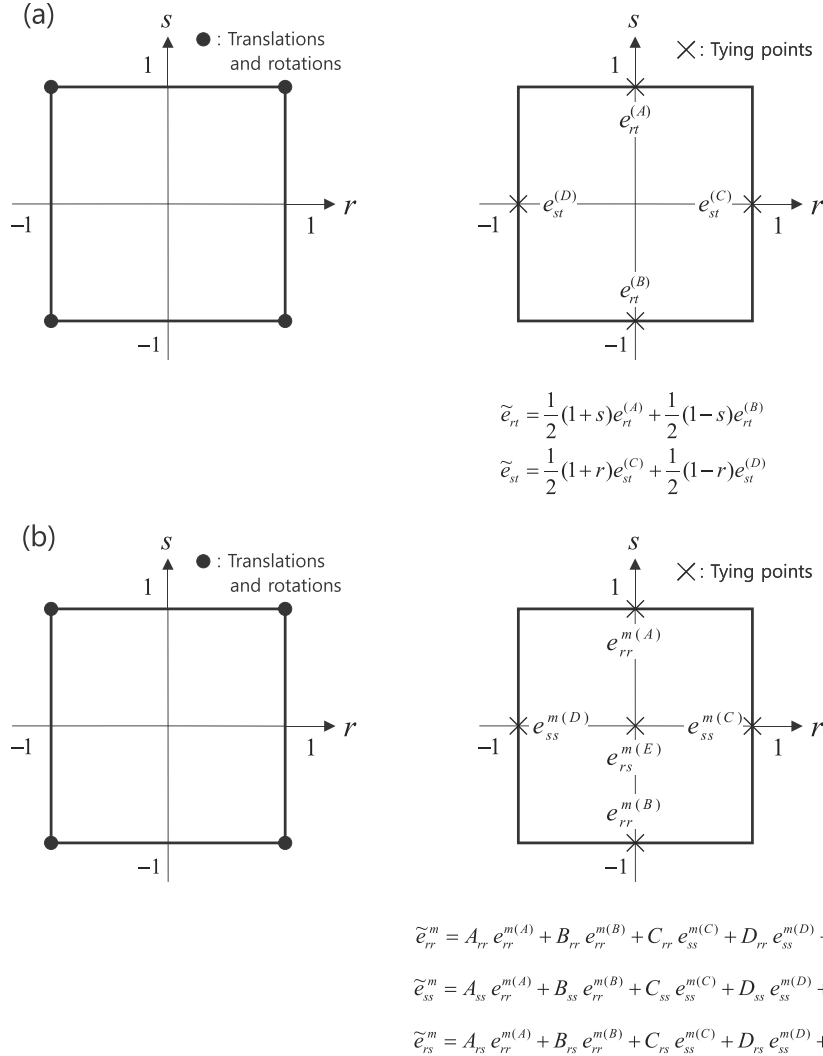


Fig. 2. The 4-node MITC shell elements. (a) The assumed transverse shear strains for the MITC4 and MITC4+ elements. (b) The assumed membrane strains for the MITC4+ element.

Table 1

Shell finite elements considered in this study.

Elements	Name	Description
Results generated in this study	3-node	MITC3+
	4-node	S4 MITC4 MITC4+
		New MITC shell element by Lee et al. [3] Shell element in ABAQUS [14] MITC shell element by Dvorkin and Bathe [10] New MITC shell element by Ko et al. [5]
Results taken from the literature	3-node	DST3 DSG3 TRIC3
		Discrete shear triangular shell element by Batoz and Katili [18] Shell element based on the discrete strain gap method by Bletzinger et al. [22] Shell element based on the natural mode method by Argyris et al. [26]
	4-node	DKQ4 DKMQ SIMO4 IBRA4 DSG4
		Discrete Kirchhoff quadrilateral shell element by Batoz et al. [17] Discrete Kirchhoff quadrilateral shell element by Katili [19] Stress resultant geometrically exact shell element by Simo et al. [20] Stress resultant shell element with drilling DOFs by Ibrahimbegović and Frey [21] Shell element based on the discrete strain gap method by Bletzinger et al. [22]

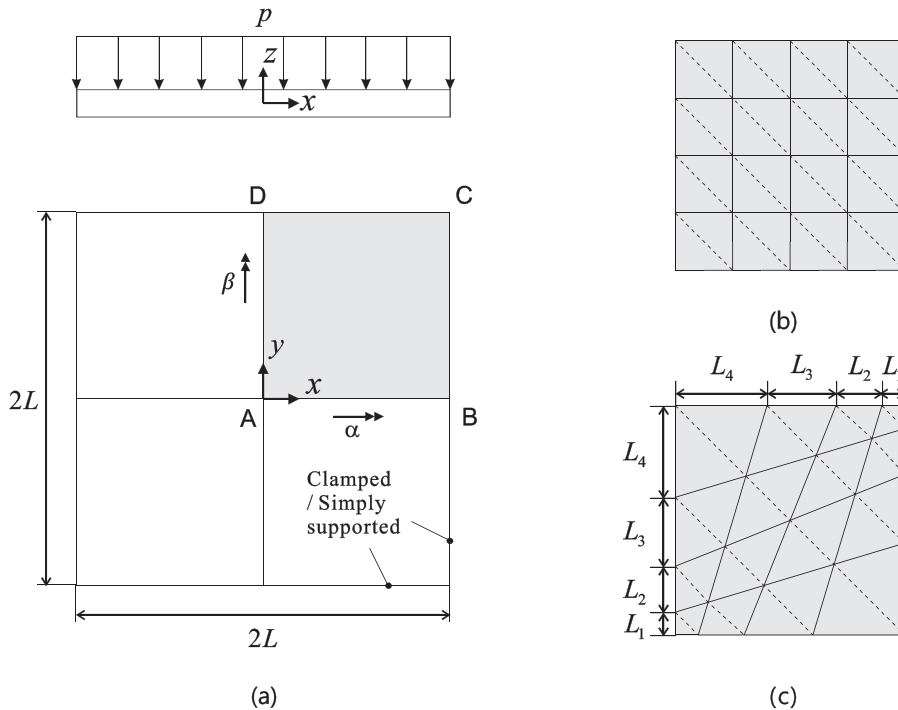


Fig. 3. Square plate problem. (a) Problem description ($L = 1.0$, thickness $t = 0.01, 0.001$ and 0.0001 , $p = 1.0 \times 10^{-2}, 1.0 \times 10^{-5}$ and 1.0×10^{-8} , $E = 1.0 \times 10^4$ and $\nu = 0.3$). (b) Regular mesh pattern ($N = 4$). (c) Distorted mesh pattern ($N = 4$, $L_1 : L_2 \dots L_N = 1 : 2 \dots N$). In (b) and (c), the solid and dotted lines denote quadrilateral and triangular elements, respectively.

widely used for many years [13]. The solution convergence is simply measured through the point-wise convergence of a displacement at a point of the shell structure. As discussed in depth in Ref. [2], this procedure to test shell elements is not stringent and does not thoroughly measure the predictive capability of shell finite elements. However, many shell finite elements previously developed have been assessed using these benchmark problems and, indeed, in new publications these tests are still frequently employed. For this reason, it is valuable to also test the new MITC shell elements using these problems, and to compare the predicted response with the results obtained using other shell elements.

In this paper, we assess the performance of the new MITC shell elements in these benchmark shell problems and give some comparisons with other shell elements previously developed. We consider various shell thicknesses and mesh distortions to identify whether shear locking or membrane locking occurs. Hence we focus on the analysis of structures, for which shear effects are small. The performance of the MITC3+ and MITC4+ shell elements

is presented by data in tables and convergence curves. The tables allow other researchers to directly compare the performance of any shell element against the elements considered here.

2. Shell finite elements

In this section, we describe the shell finite elements considered in this study. The key features of the MITC shell elements are briefly presented. For comparison, several shell elements have been selected from the literature as well as available commercial finite element software. We give here also brief descriptions of these elements.

2.1. The MITC shell elements

The key of the MITC formulation is the choice of the assumed strain fields. We briefly present the assumed strain fields used in the MITC3+, MITC4, and MITC4+ shell elements.

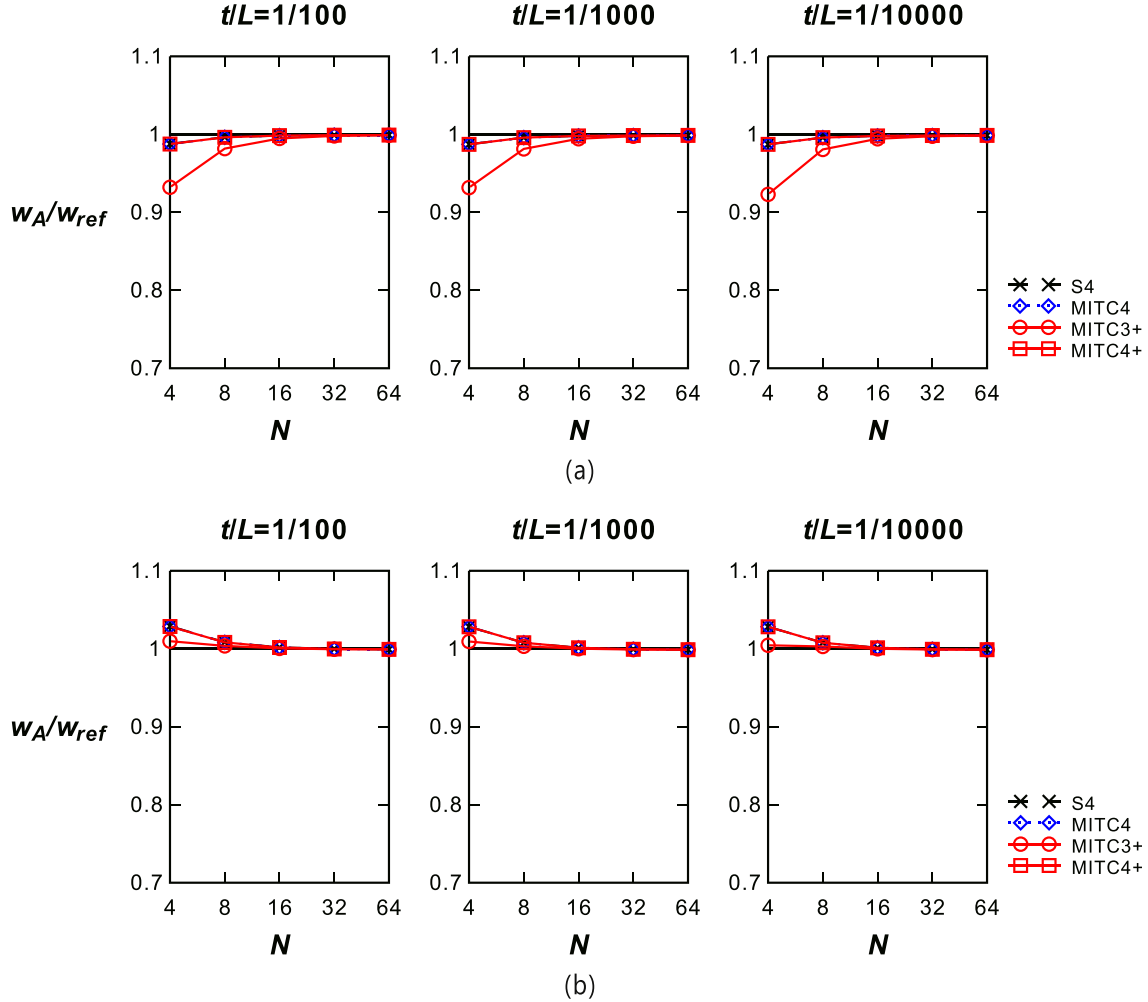


Fig. 4. Convergence of normalized displacement at point A for the clamped square plate problem with the (a) regular and (b) distorted meshes.

Table 2

Normalized displacement at the plate center (point A) for the clamped square plate problem with the regular mesh in Fig. 3(b).

t/L	N	3-node element		4-node elements		
		MITC3+	S4	MITC4	MITC4+	
1/100	4	0.9321	0.9876	0.9875	0.9875	
	8	0.9817	0.9963	0.9962	0.9962	
	16	0.9947	0.9984	0.9984	0.9984	
	32	0.9980	0.9990	0.9989	0.9989	
	64	0.9988	0.9991	0.9990	0.9990	
1/1000	4	0.9316	0.9871	0.9871	0.9871	
	8	0.9813	0.9958	0.9958	0.9958	
	16	0.9943	0.9980	0.9980	0.9980	
	32	0.9976	0.9985	0.9985	0.9985	
	64	0.9984	0.9986	0.9986	0.9986	
1/10000	4	0.9230	0.9871	0.9871	0.9871	
	8	0.9806	0.9958	0.9958	0.9958	
	16	0.9942	0.9979	0.9979	0.9979	
	32	0.9976	0.9985	0.9985	0.9985	
	64	0.9984	0.9986	0.9986	0.9986	

Reference solution: -2.2137×10^{-1}

Fig. 1 presents the basic features of the MITC3+ shell element [1,11]. The nodal degrees of freedom (DOFs), the assumed strain fields for transverse shear strains and the corresponding tying positions are given. The MITC3+ shell element has the nodal degrees-of freedom (DOFs) of standard 3-node shell elements, that

is, 5 DOFs per node and 15 DOFs in total. However, in the MITC3+ formulation two internal rotations interpolated by the cubic bubble function are used. The corresponding DOFs are condensed out on the element level. Since the geometry of the 3-node shell element is flat, membrane locking is not treated.

Table 3

Normalized displacement at the plate center (point A) for the clamped square plate problem with the distorted mesh in Fig. 3(c).

t/L	N	3-node element		4-node elements	
		MITC3+	S4	MITC4	MITC4+
1/100	4	1.010	1.029	1.029	1.029
	8	1.004	1.008	1.008	1.008
	16	1.000	1.002	1.002	1.002
	32	0.9995	0.9999	0.9998	0.9998
	64	0.9992	0.9994	0.9993	0.9993
1/1000	4	1.009	1.028	1.028	1.028
	8	1.003	1.008	1.008	1.008
	16	1.000	1.001	1.001	1.001
	32	0.9991	0.9994	0.9994	0.9994
	64	0.9988	0.9989	0.9989	0.9989
1/10000	4	1.004	1.028	1.028	1.028
	8	1.003	1.008	1.008	1.008
	16	1.000	1.001	1.001	1.001
	32	0.9990	0.9994	0.9994	0.9994
	64	0.9988	0.9988	0.9988	0.9988

Reference solution: -2.2137×10^{-1}

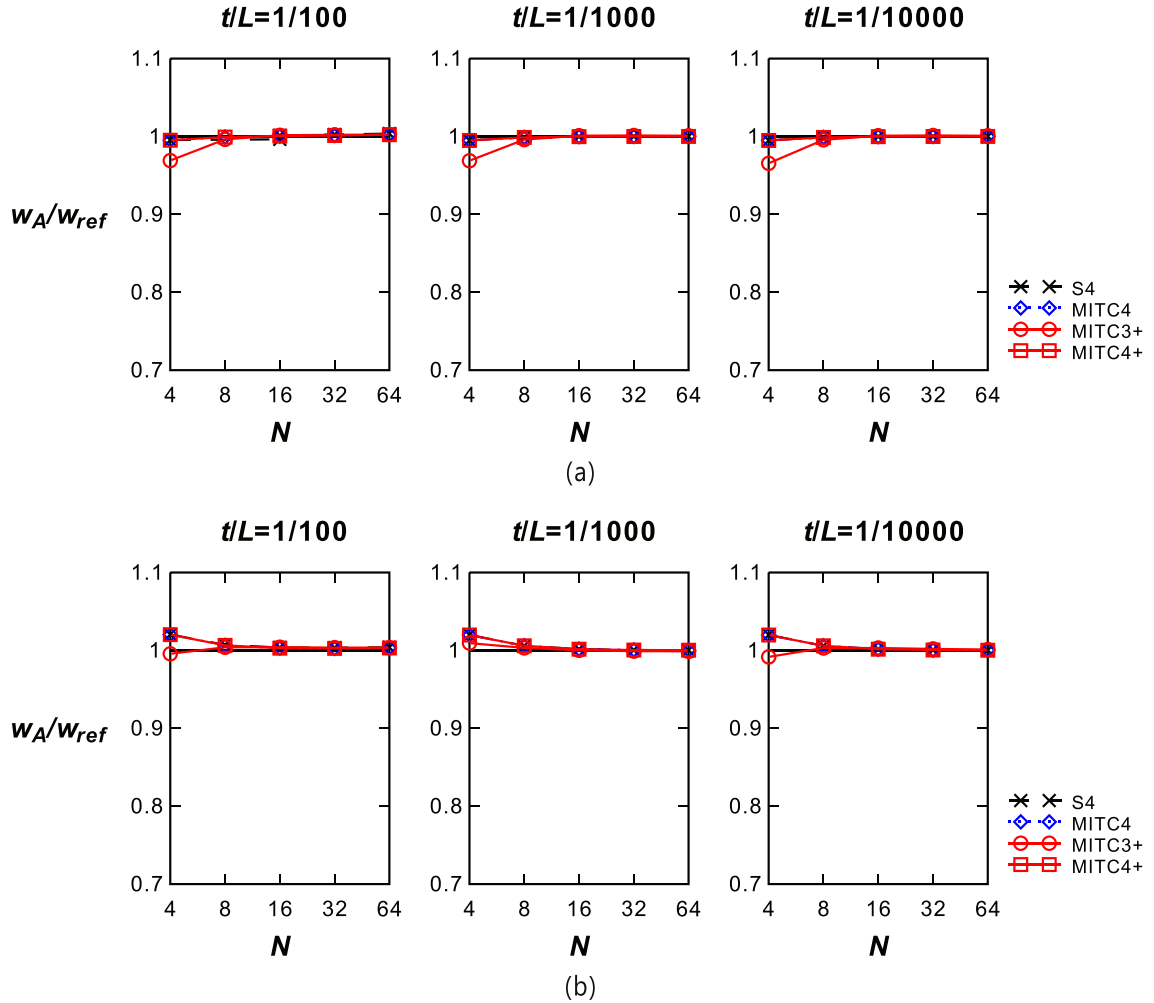


Fig. 5. Convergence of normalized displacement at point A for the simply supported square plate problem with the (a) regular and (b) distorted meshes.

In Fig. 2, we present the nodal DOFs, the assumed strain fields for the transverse shear and membrane strains and the corresponding tying positions [4,5,10]. In the MITC4 shell element, the MITC method is only employed for the transverse shear strains to alleviate shear locking. The MITC4+ shell element uses the same assumed transverse shear strain fields as the MITC4 shell element,

but also assumed membrane strains to also alleviate membrane locking. The 4-node shell elements have the nodal DOFs of standard 4-node shell elements (5 DOFs per node and 20 nodal DOFs in total). The coefficients for the assumed membrane strain fields are derived from the element geometry, see Refs. [4,5] for the details.

Table 4

Normalized displacement at the plate center (point A) for the simply supported square plate problem with the regular mesh in Fig. 3(b).

t/L	N	3-node element MITC3+	4-node elements		
			S4	MITC4	MITC4+
1/100	4	0.9690	0.9954	0.9952	0.9952
	8	0.9963	0.9997	0.9992	0.9992
	16	1.002	1.001	1.000	1.000
	32	1.002	1.003	1.001	1.001
	64	1.003	1.004	1.002	1.002
1/1000	4	0.9688	0.9949	0.9949	0.9949
	8	0.9960	0.9988	0.9988	0.9988
	16	1.001	0.9998	0.9998	0.9998
	32	1.001	1.000	1.000	1.000
	64	1.001	1.000	1.000	1.000
1/10,000	4	0.9655	0.9949	0.9949	0.9949
	8	0.9957	0.9988	0.9988	0.9988
	16	1.001	0.9998	0.9998	0.9998
	32	1.001	1.000	1.000	1.000
	64	1.001	1.000	1.000	1.000
Reference solution: -7.0971×10^{-1}					

Table 5

Normalized displacement at the plate center (point A) for the simply supported square plate problem with the distorted mesh in Fig. 3(c).

t/L	N	3-node element MITC3+	4-node elements		
			S4	MITC4	MITC4+
1/100	4	0.9957	1.020	1.020	1.020
	8	1.004	1.007	1.006	1.006
	16	1.004	1.004	1.003	1.003
	32	1.004	1.004	1.003	1.003
	64	1.004	1.004	1.003	1.003
1/1000	4	0.9953	1.020	1.020	1.020
	8	1.003	1.006	1.006	1.006
	16	1.003	1.002	1.002	1.002
	32	1.002	1.001	1.001	1.001
	64	1.001	1.000	1.000	1.000
1/10000	4	0.9917	1.020	1.020	1.020
	8	1.003	1.006	1.006	1.006
	16	1.003	1.002	1.002	1.002
	32	1.002	1.000	1.000	1.000
	64	1.001	1.000	1.000	1.000
Reference solution: -7.0971×10^{-1}					

2.2. Shell elements for comparison

We describe here briefly the shell elements selected for the comparison study. All shell elements have 5 DOFs per node unless otherwise noted.

The S4 shell element offered in ABAQUS [14] is used. The S4 element is a fully integrated 4-node shell element using the Dvorkin-Bathe transverse shear interpolation [9,10]. Hence, as shown in the example solutions below, the performance of the S4 element is like for the MITC4 shell element. For the plate solutions considered, the same results to 3 digits are obtained even when using distorted meshes, but for curved structures, due to the curvature and membrane effects, the S4 and MITC4 shell elements result in different solutions.

Based on the discrete Kirchhoff plate theory, the discrete Kirchhoff triangular (DKT) 3-node shell element [15,16] and the discrete Kirchhoff quadrilateral 4-node shell element (DKQ4) [17] were developed. These elements are known to accurately represent thin-plate limit solutions. The 3-node and 4-node shell elements were extended to include the effect of transverse shear deformations, resulting in the DST3 [18] and DKMQ [19] elements, respectively. The DKMQ element also uses the Dvorkin-Bathe transverse shear interpolation.

We also consider the stress resultant 4-node shell elements developed by Simo et al. [20] and by Ibrahimbegović and Frey [21], which are denoted as SIMO4 and IBRA4, respectively. For the formulation of the SIMO4 shell element, the Hellinger-Reissner principle was used for the in-plane strains and the assumed strain method was used for the transverse shear strains. For the IBRA4 element, the incompatible mode technique and the assumed strain method were used for the in-plane strains and the transverse shear strains, respectively. The element includes the drilling degrees of freedom and thus the IBRA4 element has 6 DOFs per node. Both elements use the Dvorkin-Bathe transverse shear interpolation scheme.

The DSG discrete shear gap method was developed by Bletzinger et al. for reducing shear locking [22] and the 3-node and 4-node DSG shell elements were proposed. The DSG3 element does not satisfy the isotropy condition and thus the behavior of the element depends on the node numbering sequence used [22,23]. The DSG4 element formulation gives the MITC4 element when used for plates. The DSG method was later applied to alleviate membrane locking of the 4-node shell element [24] but the resulting element fails to pass the patch tests.

The NM (Natural Mode) method has been successfully employed, in particular for the development of 3-node triangular

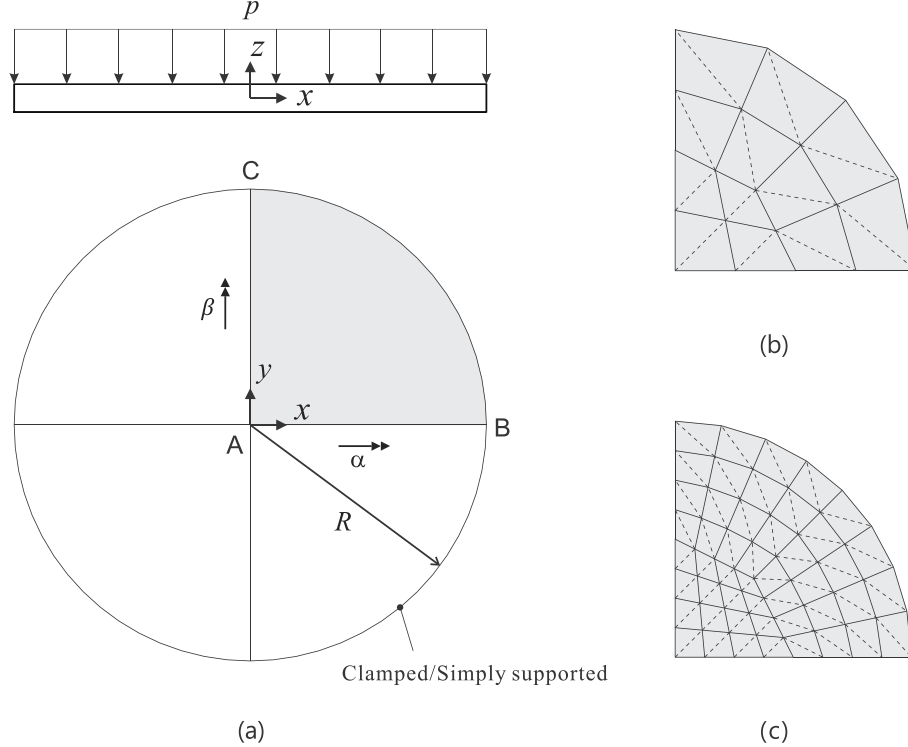


Fig. 6. Circular plate problem. (a) Problem description ($R = 1.0$, thickness $t = 0.01, 0.001$ and 0.0001 , $p = 1.0 \times 10^{-2}, 1.0 \times 10^{-5}$ and 1.0×10^{-8} , $E = 1.0 \times 10^4$ and $\nu = 0.3$). (b) Mesh with $N = 4$. (c) Mesh with $N = 8$. In (b) and (c), the solid and dotted lines denote quadrilateral and triangular element meshes, respectively.

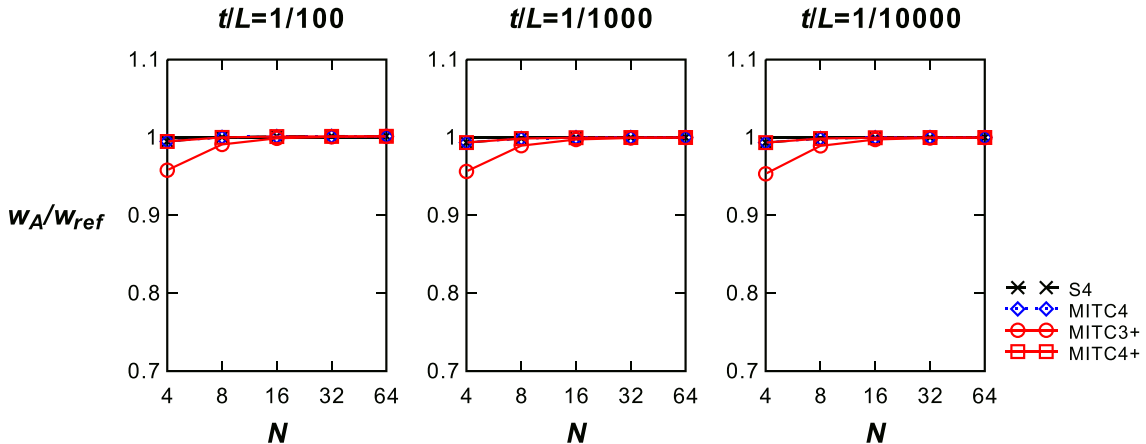


Fig. 7. Convergence of normalized displacement at point A for the clamped circular plate problem.

plate and shell elements [25,26]. The method assumes rigid-body, constant and higher-order straining modes naturally arising from the element geometry. The 3-node TRIC shell element is considered to be the best of this kind [26].

Table 1 lists the shell elements considered. The S4, MITC4, MITC3+ and MITC4+ shell elements are in this study tested (ABAQUS is used to test the S4 element) whereas the results for the other shell elements are simply quoted from given data in publications. However, results using distorted meshes of the elements in the literature have largely not been published and hence such results are not given in this paper. Thus, without programming these elements, we cannot see whether these elements lock when distorted meshes are employed.

We use for the in-plane integration 3-point Gauss integration for the MITC3+ shell element and 2×2 Gauss integration for the

S4, MITC4 and MITC4+ shell elements. In all cases, we use 2-point Gauss integration in the thickness direction.

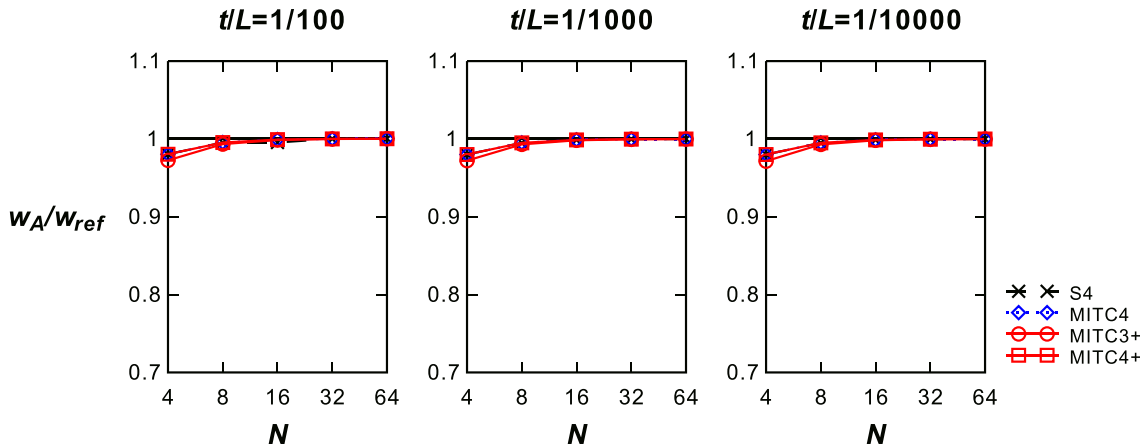
3. Solutions of benchmark problems

In this section, we present the results of several test problems which have been widely adopted for the evaluation of shell elements: square and circular plate problems, the pinched cylinder problem, the Scordelis-Lo roof problem, the twisted beam problems, a hemispherical shell problem, a full hemisphere shell problem and a hyperbolic paraboloid shell problem [1–6,8–13,15–30]. For the convergence studies, the results of the displacement solutions are given both in tabular form and convergence graphs to facilitate the use of the results in future works. In particular,

Table 6

Normalized displacement at the plate center (point A) for the clamped circular plate problem.

t/L	N	3-node elements			4-node elements			
		MITC3+	DST3	DSG3	S4	MITC4	MITC4+	DSG4
1/100	4	0.9580	–	–	0.9949	0.9949	0.9949	–
	8	0.9910	–	–	1.000	1.000	1.000	–
	16	0.9989	–	–	1.002	1.001	1.001	–
	32	1.001	–	–	1.002	1.001	1.001	–
	64	1.001	–	–	1.002	1.002	1.002	–
1/1000	4	0.9564	1.020	0.9621	0.9934	0.9934	0.9934	0.9927
	8	0.9895	1.006	0.9908	0.9986	0.9986	0.9986	0.9985
	16	0.9974	1.001	0.9978	0.9997	0.9997	0.9997	0.9997
	32	0.9994	–	–	0.9999	0.9999	0.9999	–
	64	0.9999	–	–	1.000	1.000	1.000	–
1/10,000	4	0.9534	–	–	0.9934	0.9934	0.9934	–
	8	0.9893	–	–	0.9986	0.9986	0.9986	–
	16	0.9974	–	–	0.9997	0.9997	0.9997	–
	32	0.9994	–	–	0.9999	0.9999	0.9999	–
	64	0.9998	–	–	1.000	1.000	1.000	–

Reference solution: -2.1328×10^{-2} **Fig. 8.** Convergence of normalized displacement at point A for the simply supported circular plate problem.**Table 7**

Normalized displacement at the plate center (point A) for the simply supported circular plate problem.

t/L	N	3-node element		4-node elements			DKMQ
		MITC3+	S4	MITC4	MITC4+	DKMQ	
1/100	4	0.9725	0.9803	0.9803	0.9803	0.9900	–
	8	0.9934	0.9954	0.9954	0.9954	0.9976	–
	16	0.9986	0.9992	0.9991	0.9991	–	–
	32	0.9999	1.000	1.000	1.000	–	–
	64	1.000	1.000	1.000	1.000	–	–
1/1000	4	0.9721	0.9800	0.9800	0.9800	–	–
	8	0.9930	0.9950	0.9950	0.9950	–	–
	16	0.9983	0.9988	0.9988	0.9988	–	–
	32	0.9996	0.9997	0.9997	0.9997	–	–
	64	0.9999	0.9999	0.9999	0.9999	–	–
1/10000	4	0.9714	0.9800	0.9800	0.9800	–	–
	8	0.9929	0.9950	0.9950	0.9950	–	–
	16	0.9982	0.9988	0.9988	0.9988	–	–
	32	0.9996	0.9997	0.9997	0.9997	–	–
	64	0.9999	0.9999	0.9999	0.9999	–	–

Reference solution: -8.6953×10^{-2}

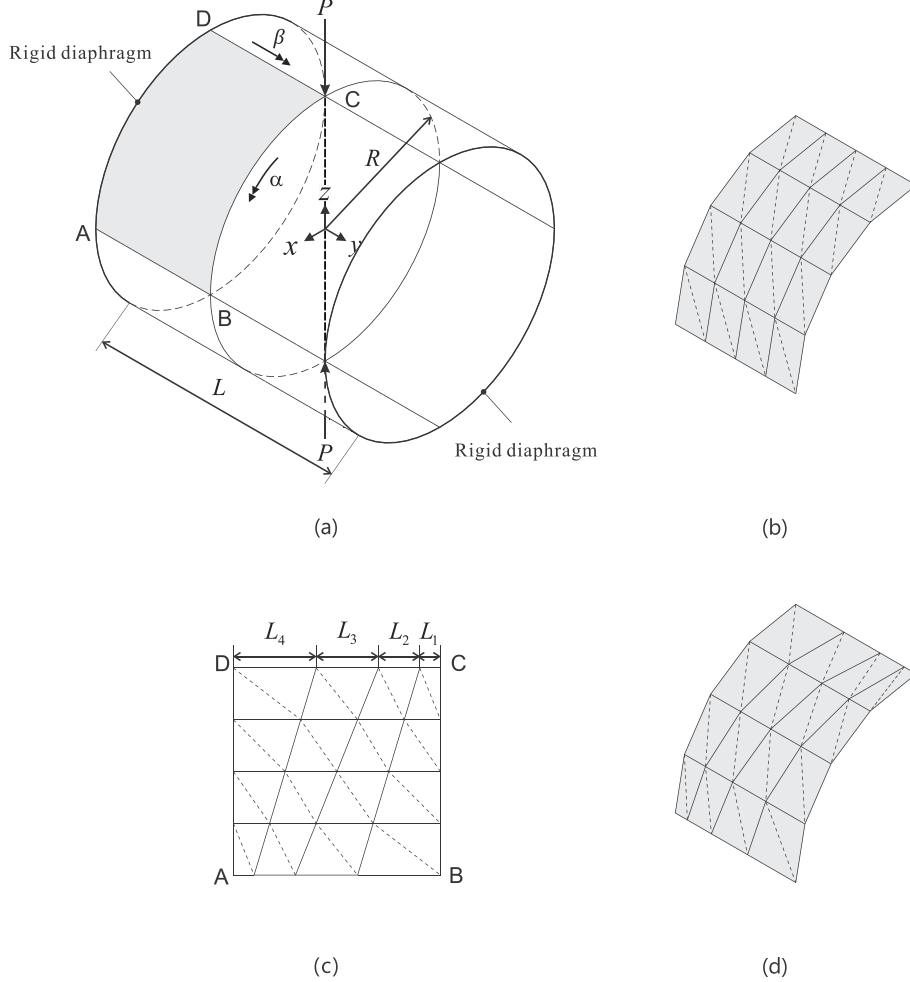


Fig. 9. Pinched cylinder problem. (a) Problem description ($L = 600$, $R = 300$, thickness $t = 3.0$, $P = 1.0$, $E = 3.0 \times 10^6$ and $\nu = 0.3$). (b) The regular mesh with $N = 4$. (c) Distorted mesh pattern. (d) The distorted mesh with $N = 4$. In (b) and (d), the solid and dotted lines denote quadrilateral and triangular element meshes, respectively.

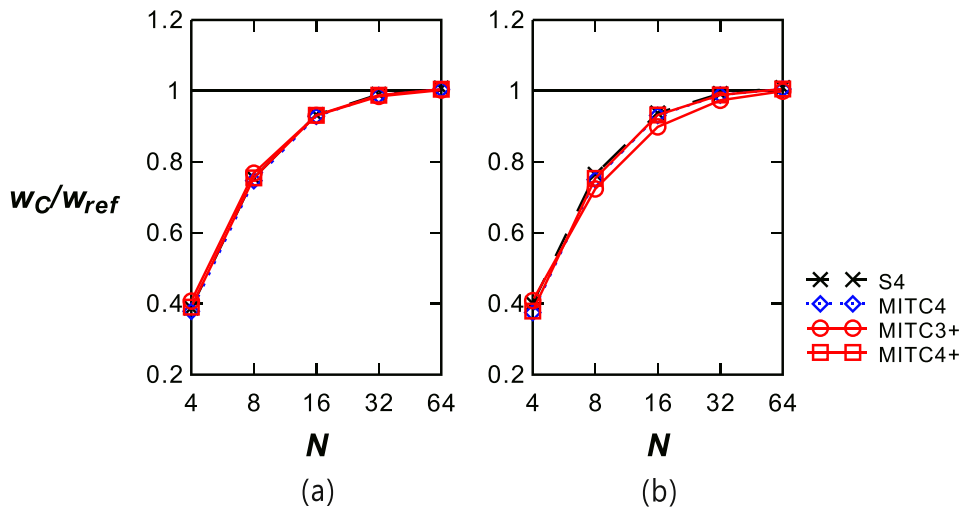


Fig. 10. Convergence of normalized displacement at point C for the pinched cylinder problem with the (a) regular and (b) distorted meshes.

solutions with distorted meshes are also presented for the S4, MITC4, MITC3+ and MITC4+ shell elements.

For describing the displacement boundary conditions, we use the notation u , v and w to denote the translational displacements

in the global x , y and z directions. While the two local rotations α and β are used for the MITC4, MITC3+ and MITC4+ shell elements, the global rotations θ_x , θ_y and θ_z (about the global x , y and z axes, respectively) are used for the S4 shell element in ABAQUS.

Table 8

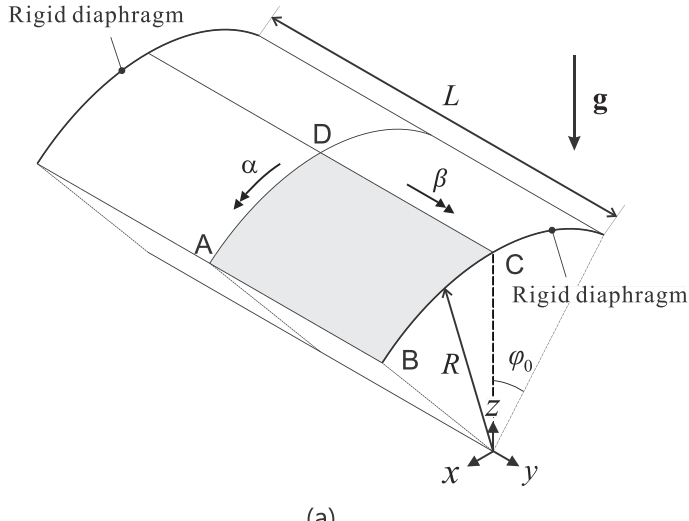
Normalized displacement at the point of load application (point C) for the pinched cylinder problem with the regular mesh in Fig. 9(b).

N	3-node elements		4-node elements					
	MITC3+	TRIC3	S4	MITC4	MITC4+	SIM04	DKQ4	IBRA4
4	0.4074	0.394	0.3882	0.3788	0.3904	0.399	0.636	0.3700
8	0.7681	0.778	0.7544	0.7469	0.7548	0.763	0.951	0.7367
16	0.9308	0.953	0.9328	0.9286	0.9313	0.934	1.016	0.9343
32	0.9847	–	0.9902	0.9871	0.9878	–	–	–
64	1.002	–	1.008	1.005	1.005	–	–	–
Reference solution: -1.8248×10^{-5}								

Table 9

Normalized displacement at the point of load application (point C) for the pinched cylinder problem with the distorted mesh in Fig. 9(d).

N	3-node element		4-node elements		
	MITC3+	S4	MITC4	MITC4+	
4	0.4088	0.4010	0.3751	0.3793	
8	0.7237	0.7647	0.7498	0.7535	
16	0.8986	0.9375	0.9308	0.9321	
32	0.9734	0.9924	0.9882	0.9886	
64	0.9992	1.009	1.005	1.005	
Reference solution: -1.8248×10^{-5}					



(a)

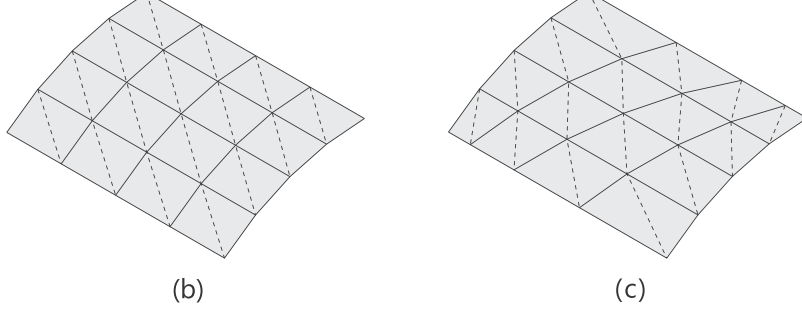


Fig. 11. Scordelis-Lo roof problem. (a) Problem description ($L = 50$, $R = 25$, $\varphi_0 = 40^\circ$, thickness $t = 0.25$, density $\rho = 360$, acceleration of gravity \mathbf{g} with magnitude 1.0, $E = 4.32 \times 10^8$ and $v = 0.0$). (b) The regular mesh with $N = 4$. (c) The distorted mesh in Fig. 9(c) used here ($N = 4$). In (b) and (c), the solid and dotted lines denote quadrilateral and triangular element meshes, respectively.

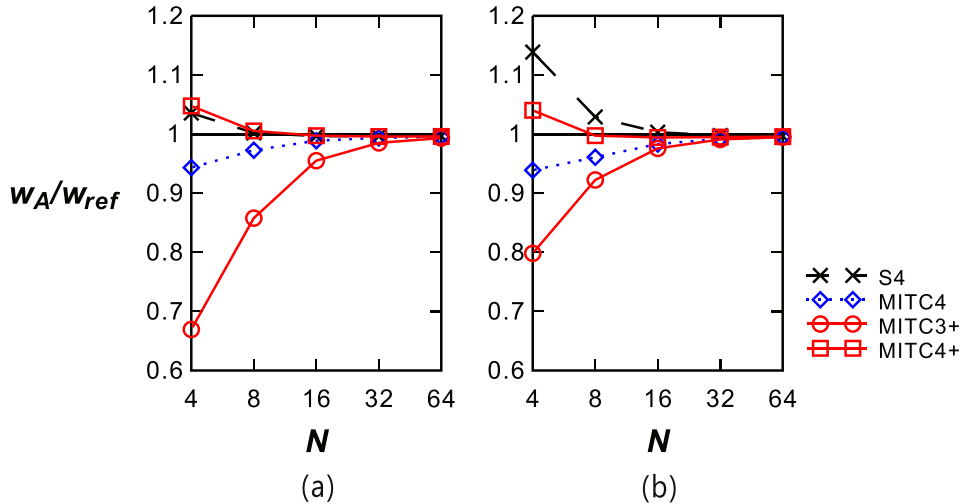


Fig. 12. Convergence of normalized displacement at point A for the Scordelis-Lo roof problem with the (a) regular and (b) distorted meshes.

Table 10

Normalized displacement at the center of the free edge (point A) for the Scordelis-Lo roof problem with the regular mesh in Fig. 11(b).

N	3-node elements		4-node elements					
	MITC3+	TRIC3	S4	MITC4	MITC4+	SIMO4	DKQ4	IBRA4
4	0.6695	0.697	1.036	0.9432	1.048	1.083	1.048	1.047
8	0.8577	0.902	1.002	0.9726	1.005	1.015	1.005	1.005
16	0.9550	—	0.9966	0.9886	0.9973	1.000	0.996	0.9974
32	0.9851	—	0.9961	0.9936	0.9958	—	—	—
64	0.9932	—	0.9965	0.9955	0.9960	—	—	—
Reference solution: -3.0240×10^{-1}								

Table 11

Normalized displacement at the center of the free edge (point A) for the Scordelis-Lo roof problem with the distorted mesh in Fig. 11(c).

N	3-node element		4-node elements		
	MITC3+	S4	MITC4	MITC4+	
4	0.7982	1.139	0.9389	1.040	
8	0.9223	1.029	0.9607	0.9973	
16	0.9757	1.003	0.9831	0.9942	
32	0.9909	0.9975	0.9919	0.9948	
64	0.9948	0.9967	0.9949	0.9957	
Reference solution: -3.0240×10^{-1}					

Following the earlier publications, in some problems concentrated point loads are applied to the structure and in all problems the displacement at only a point is measured to identify the convergence behavior. This is not a mathematically well-founded and stringent procedure, as discussed in detail in Refs. [1,2,12], but to enable the comparisons we need to proceed in that way and the results are of course still valuable.

3.1. Square plate problems

We solve the bending problem of the square plate shown in Fig. 3(a). A uniformly distributed load of pressure p is applied to the plate with clamped or simply supported boundary conditions along its four edges. Due to symmetry, one-quarter of

the plate corresponding to the shaded region ABCD in Fig. 3(a) is modeled. The boundary conditions are $u = \beta = 0$ ($u = \theta_y = \theta_z = 0$) along AD, $v = \alpha = 0$ ($v = \theta_x = \theta_z = 0$) along AB. Along BC and CD, $u = v = w = \alpha = \beta = 0$ ($u = v = w = \theta_x = \theta_y = \theta_z = 0$) for the clamped case, and $u = v = w = 0$ for the simply supported case.

The solutions are obtained using $N \times N$ element meshes ($N = 4, 8, 16, 32$, and 64). In addition to the regular mesh pattern in Fig. 3(b), we also consider the distorted mesh pattern in Fig. 3(c) such that each edge is discretized in the following ratio: $L_1:L_2:L_3: \dots L_N = 1:2:3: \dots N$ for an $N \times N$ element mesh.

In this bending-dominated problem, we consider the thickness to length ratios $t/L = 1/100, 1/1000$ and $1/10000$. The corresponding applied load magnitudes are $p = 1.0 \times 10^{-2}, 1.0 \times 10^{-5}$ and

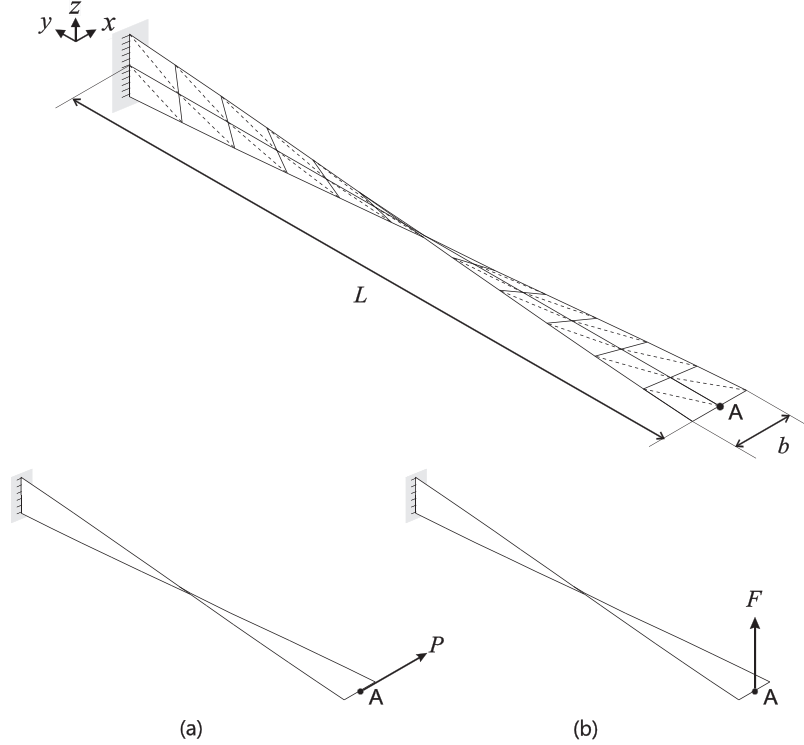


Fig. 13. Twisted beam problem (2×12 mesh, $L = 12.0$, $b = 1.1$, thickness $t = 0.32$ and 0.0032 , $P = F = 1.0$ and $P = F = 1.0 \times 10^{-6}$, $E = 29.0 \times 10^6$ and $\nu = 0.22$) with the (a) in-plane and (b) out-of-plane load cases. The solid and dotted lines denote quadrilateral and triangular element meshes, respectively.

1.0×10^{-8} . The following reference displacements at the plate center (point A) obtained using the Kirchhoff thin plate theory are used [27]:

$$\begin{aligned} w_{ref} &= -1.267 \times 10^{-3} \frac{pL^4}{D} \quad \text{for the clamped case,} \\ w_{ref} &= -4.062 \times 10^{-3} \frac{pL^4}{D} \quad \text{for the simply supported case} \end{aligned} \quad (1)$$

with the bending rigidity $D = \frac{Et^3}{12(1-\nu^2)}$.

Fig. 4 and **Tables 2–3** show the convergence of the normalized displacement (w_A/w_{ref}) at the plate center for the clamped square plate problem with regular and distorted meshes. **Fig. 5** and **Tables 4–5** present these results when considering the simply supported plate. All considered shell elements perform in this analysis very well in both the regular and distorted meshes, and the S4 and MITC4 element results are the same to 3 digits because, for plates, the S4 element seems to be the MITC4 element.

3.2. Circular plate problems

We consider the circular plate shown in **Fig. 6(a)**. The uniformly distributed load with pressure p is applied to the plate with clamped and simply supported boundary conditions along its edges. Utilizing symmetry, only one-quarter of the plate corresponding to the shaded region ABC in **Fig. 6(a)** is modeled. The boundary conditions are $u = \beta = 0$ ($u = \theta_y = \theta_z = 0$) along AC, and $\nu = \alpha = 0$ ($\nu = \theta_x = \theta_z = 0$) along AB. Along BC, $u = \nu = w = \alpha = \beta = 0$ ($u = \nu = w = \theta_x = \theta_y = \theta_z = 0$) for the clamped case, and $u = \nu = w = 0$ for the simply supported case. The solutions are obtained using N elements per edge with $N = 4, 8, 16, 32$ and 64 .

The thickness to length ratios used are $t/L = 1/100, 1/1000$ and $1/10,000$ ($L = 2R$), where the applied load magnitudes are varied to be $p = 1.0 \times 10^{-2}, 1.0 \times 10^{-5}$ and 1.0×10^{-8} . The reference displacements at the plate center (point A) are given as follows [27]:

$$\begin{aligned} w_{ref} &= -\frac{pR^4}{64D} \quad \text{for the clamped case,} \\ w_{ref} &= -\frac{pR^4}{64D} \cdot \frac{5+\nu}{1+\nu} \quad \text{for the simply supported case,} \end{aligned} \quad (2)$$

which are based on the Kirchhoff thin plate theory.

Fig. 7 and **Table 6**, and **Fig. 8** and **Table 7** present the convergence of the normalized displacement (w_A/w_{ref}) at the plate center for the clamped and simply supported plate problems, respectively. The MITC3+ and MITC4+ shell elements show excellent convergence behavior in the entire range of thickness to length ratios considered.

3.3. Pinched cylinder problem

The pinched cylinder with rigid end diaphragms shown in **Fig. 9(a)** is considered. The structure is subjected to a pair of pinching forces P . One-eighth of the cylinder corresponding to the shaded region ABCD in **Fig. 9(a)** is modeled for the analysis. The boundary conditions are $u = \beta = 0$ ($u = \theta_y = \theta_z = 0$) along CD, $w = \beta = 0$ ($w = \theta_x = \theta_y = 0$) along AB, $\nu = \alpha = 0$ ($\nu = \theta_x = \theta_z = 0$) along BC, and $u = w = \beta = 0$ ($u = w = \theta_y = 0$) along AD.

The solutions are obtained using $N \times N$ element meshes ($N = 4, 8, 16, 32$, and 64). In addition to the regular mesh pattern in **Fig. 9(b)**, the distorted mesh pattern in **Fig. 9(c)** is employed where edges AB and CD are discretized in the following ratio: $L_1:L_2:L_3: \dots L_N = 1:2:3: \dots N$ for an $N \times N$ element mesh. The used distorted mesh is shown in **Fig. 9(d)**. The reference displacement at the position of load, point C, is $w_{ref} = -1.8248 \times 10^{-5}$ [28].

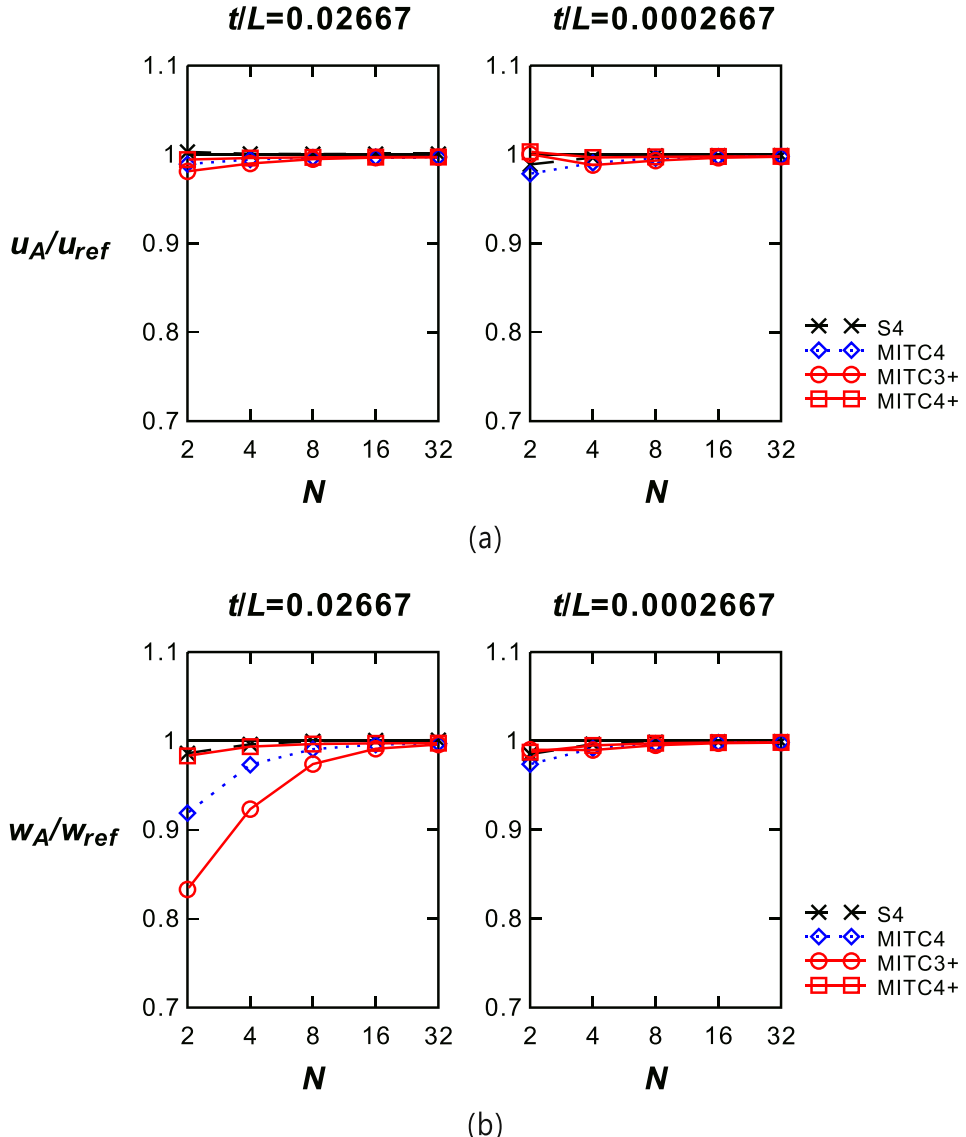


Fig. 14. Convergence of normalized displacements at point A for the twisted beam problem with (a) in-plane and (b) out-of-plane loads.

Table 12

Normalized horizontal displacement at the tip center (point A) for the twisted beam under in-plane load.

Table 13

Normalized vertical displacement at the tip center (point A) for the twisted beam under out-of-plane load.

t/L	N	3-node element	4-node elements			
		MITC3+	S4	MITC4	MITC4+	IBRA4
0.02667	2	0.8329	0.9862	0.9188	0.9832	1.0000
	4	0.9233	0.9962	0.9732	0.9936	0.9994
	8	0.9740	0.9996	0.9907	0.9965	–
	16	0.9912	1.001	0.9959	0.9973	–
	32	0.9960	1.001	0.9972	0.9975	–
	Reference solution: 1.7540×10^{-3}					
0.0002667	2	0.9901	0.9852	0.9738	0.9874	–
	4	0.9898	0.9964	0.9917	0.9949	–
	8	0.9951	0.9986	0.9967	0.9975	–
	16	0.9975	0.9991	0.9980	0.9982	–
	32	0.9982	0.9992	0.9983	0.9984	–
	Reference solution: 1.2940×10^{-3}					

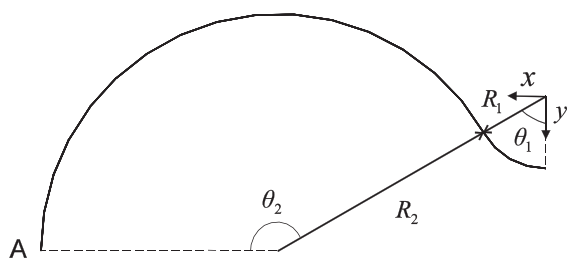
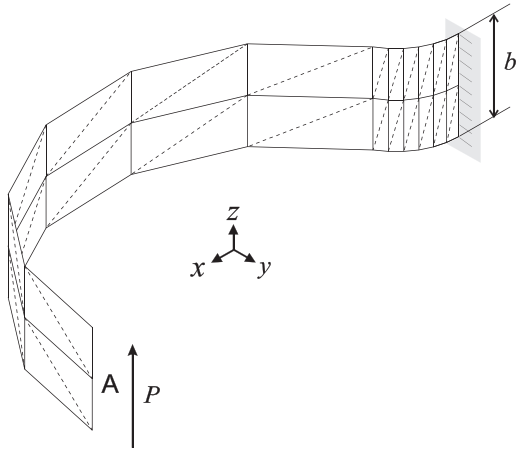


Fig. 15. Hook problem (2×12 mesh, $R_1 = 14$, $\theta_1 = 60^\circ$, $R_2 = 46$, $\theta_2 = 150^\circ$, $b = 20$, thickness $t = 2.0$, $P = 1.0$, $E = 3.3 \times 10^3$ and $v = 0.3$). The solid and dotted lines denote quadrilateral and triangular element meshes, respectively.

Fig. 10 and **Tables 8–9** present the convergence of the normalized displacement (w_C/w_{ref}) at the location of the pinching force. The MITC3+ and MITC4+ shell elements provide solutions comparable to those obtained with the other shell elements considered in this study.

3.4. Scordelis-Lo roof problem

The Scordelis-Lo roof problem is shown in **Fig. 11(a)**. The cylindrical roof structure supported by rigid diaphragms at both ends is subjected to its self-weight. Only one-quarter of the roof structure corresponding to the shaded region ABCD in **Fig. 11(a)** is modeled.

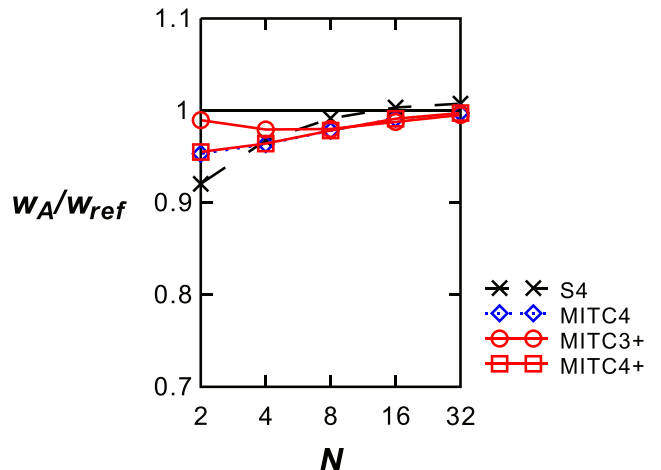


Fig. 16. Convergence of normalized displacement at point A for the hook problem.

The boundary conditions are $u = \beta = 0$ ($u = \theta_y = \theta_z = 0$) along CD, $v = \alpha = 0$ ($v = \theta_x = \theta_z = 0$) along AD, and $u = w = \beta = 0$ ($u = w = \theta_y = 0$) along BC.

The solutions are obtained using $N \times N$ element meshes ($N = 4, 8, 16, 32$, and 64). The regular and distorted mesh patterns in **Fig. 9(b)** and **(c)** are again used as shown in **Fig. 11(b)** and **(c)**, respectively. The reference displacement at the center of the free edge (point A) is $w_{ref} = -0.3024$ [28].

Fig. 12 and **Tables 10–11** present the convergence of the normalized displacement (w_A/w_{ref}) at the center of the free edge. This shell is known to be subjected to a mixed membrane-bending behavior [6]. The MITC3+ and MITC4+ shell elements show a good performance.

3.5. Twisted beam problems

We solve the twisted beam problems shown in **Fig. 13**. The initially twisted beam is fully clamped at one end and is loaded by a point load at the center of the free tip (point A). Two load cases are considered: an in-plane and an out-of-plane load as shown in **Fig. 13(a)** and **(b)**. We use $N \times 6N$ meshes with $N = 2, 4, 8, 16$, and 32 . Two thickness to length ratios $t/L = 0.02667$ and 0.0002667 are considered, where the corresponding load magnitudes are varied as $F = P = 1.0$ and $F = P = 1.0 \times 10^{-6}$, respectively.

Table 14

Normalized displacement at the point of load application (point A) for the hook problem.

N	3-node element	4-node elements		
	MITC3+	S4	MITC4	MITC4+
2	0.9896	0.9204	0.9531	0.9531
4	0.9794	0.9675	0.9635	0.9635
8	0.9800	0.9915	0.9782	0.9782
16	0.9877	1.003	0.9911	0.9911
32	0.9952	1.008	0.9973	0.9973
Reference solution: 4.82482				

When $t/L = 0.02667$, the reference displacements at point A are $w_{ref} = 1.754 \times 10^{-3}$ and $u_{ref} = 5.424 \times 10^{-3}$ for the out-of-plane and in-plane load cases, respectively. When $t/L = 0.0002667$, the reference displacements are $w_{ref} = 1.294 \times 10^{-3}$ and $u_{ref} = 5.256 \times 10^{-3}$ for the out-of-plane and in-plane load cases, respectively [29].

Fig. 14(a) and Table 12, and Fig. 14(b) and Table 13 show the convergence of the normalized displacements (u_A/u_{ref} and w_A/w_{ref}) at the tip center for the in-plane and out-of-plane load cases, respectively. The considered elements perform well, including the MITC3+ and MITC4+ shell elements.

3.6. Hook problem

The hook problem shown in Fig. 15 is considered [30]. The structure is fully clamped at one end and is loaded by a shear load P applied as a uniformly distributed traction at its tip. We use $N \times 6N$ element meshes with $N = 2, 4, 8, 16, 32$ and each circular arc modeled by one half of the total mesh. The reference displacement at point A is $w_{ref} = 4.82482$, obtained using the MITC9 shell element with $N = 64$. Fig. 16 and Table 14 show the convergence of the normalized displacement (w_A/w_{ref}) at the tip (point A). A good convergence is observed for the solutions using the MITC3+ and MITC4+ shell elements.

3.7. Hemispherical shell with cut-out problem

We consider the hemispherical shell problem shown in Fig. 17. The hemispherical shell with an opening at its top is subjected to two pairs of radial forces along its equator. Using symmetry, one-quarter of the structure corresponding to the shaded region ABCD in Fig. 17(a) is modeled, with the following boundary conditions: $u = \beta = 0$ ($u = \theta_y = \theta_z = 0$) along BC, $v = \beta = 0$ ($v = \theta_x = \theta_z = 0$) along AD, and $w = 0$ at point A.

The solutions are obtained using $N \times N$ element meshes ($N = 4, 8, 16, 32$, and 64). The regular and distorted mesh patterns in Fig. 3 (b) and (c) are considered as shown in Fig. 17(b) and (c), respectively.

In this bending-dominated, doubly-curved shell problem, we consider two different thickness to length ratios, $t/L = 4/1000$ and $4/10,000$ ($L = R$), and the corresponding load magnitudes are $P = 2.0$ and 2.0×10^{-3} , respectively. The same reference displacement of $u_{ref} = 0.093$ at point A can be used for the test cases [20].

Fig. 18 and Tables 15–16 present the convergence of the normalized displacement (u_A/u_{ref}) at point A. When the regular meshes are used, the MITC3+, MITC4, MITC4+ and S4 shell elements show an excellent performance. However, with the distorted meshes, the solutions using the MITC4 and S4

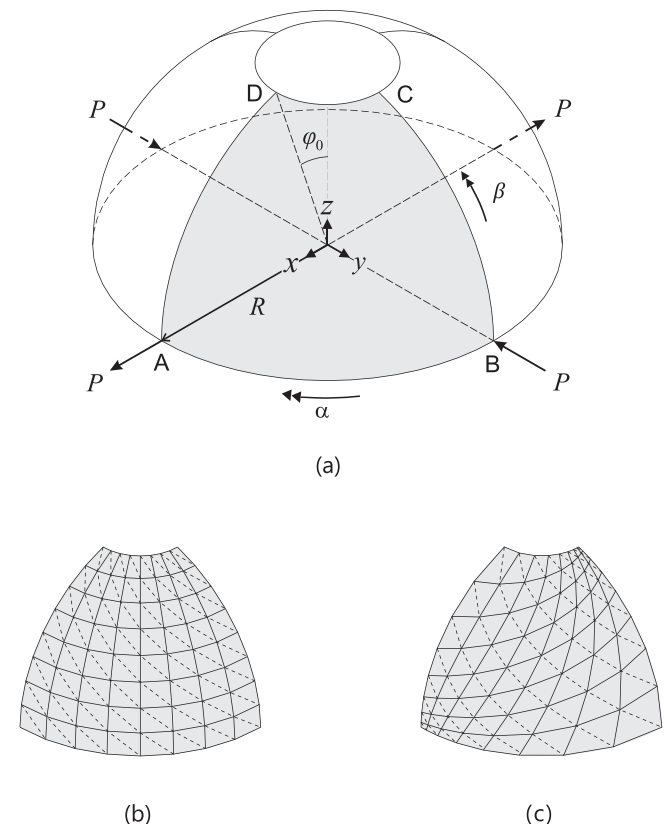


Fig. 17. Hemispherical shell with cut-out problem. (a) Problem description ($R = 10.0$, $\phi_0 = 18^\circ$, thickness $t = 0.04$ and 0.004 , $P = 2.0$ and 2.0×10^{-3} , $E = 6.825 \times 10^7$ and $v = 0.3$). (b) The regular mesh with $N = 8$. (c) The distorted mesh in Fig. 3(c) used here ($N = 8$). In (b) and (c), the solid and dotted lines denote quadrilateral and triangular element meshes, respectively.

shell elements are in large error while the MITC3+ and MITC4+ shell elements continue to provide good response predictions.

3.8. Full hemisphere problem

The shell problem considering a full hemisphere is shown in Fig. 19. The hemisphere is subjected to two pairs of radial forces along its equator. Due to symmetry, only one-quarter of the structure corresponding to the shaded region ABC in Fig. 19(a) is modeled, with the following boundary conditions: $u = \beta = 0$ ($u = \theta_y = \theta_z = 0$) along BC, $v = \beta = 0$ ($v = \theta_x = \theta_z = 0$) along AC, and $w = 0$ at point A. The solutions are obtained using N elements per edge with $N = 4, 8, 16, 32$, and 64.

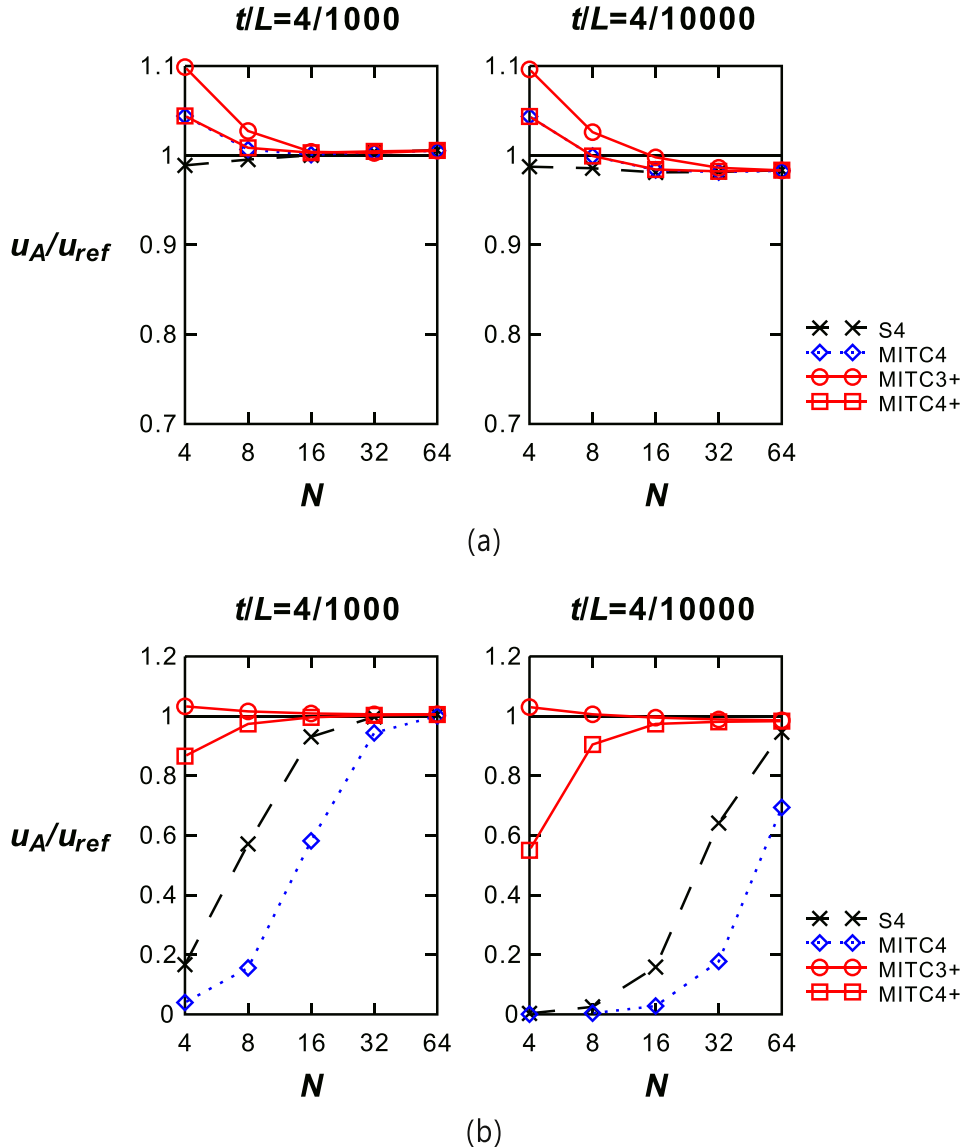


Fig. 18. Convergence of normalized displacement at point A for the hemispherical shell with cut-out problem with the (a) regular and (b) distorted meshes.

Table 15

Normalized displacement at the point of load application (point A) for the hemispherical shell with cut-out problem with the regular mesh in Fig. 17(b).

t/R	N	3-node element		4-node elements				
		MITC3+	S4	MITC4	MITC4+	SIMO4	DKQ4	IBRA4
4/1000	4	1.099	0.9889	1.044	1.044	1.004	0.928	1.011
	8	1.027	0.9954	1.007	1.009	0.998	1.010	1.002
	16	1.004	1.000	1.001	1.003	0.999	1.003	1.001
	32	1.003	1.004	1.004	1.005	–	–	–
	64	1.005	1.006	1.005	1.006	–	–	–
4/10000	4	1.096	0.9875	1.044	1.044	–	–	–
	8	1.026	0.9857	0.9993	0.9994	–	–	–
	16	0.9979	0.9811	0.9838	0.9834	–	–	–
	32	0.9863	0.9816	0.9815	0.9823	–	–	–
	64	0.9832	0.9835	0.9829	0.9836	–	–	–

Reference solution: 9.3000×10^{-2}

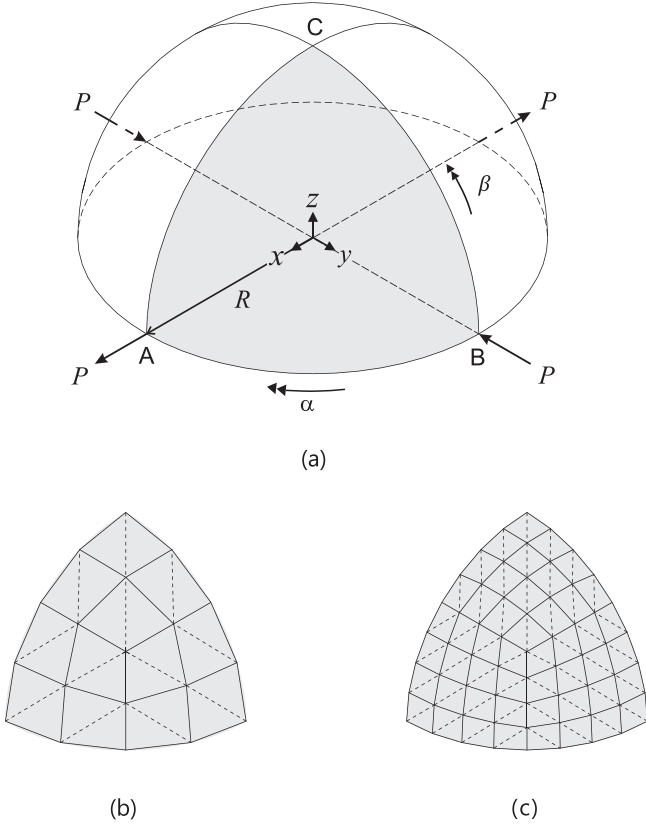


Fig. 19. Full-hemisphere shell problem. (a) Problem description ($R = 10$, thickness $t = 0.04$ and 0.004 , $P = 2.0$ and 2.0×10^{-3} , $E = 6.825 \times 10^7$ and $\nu = 0.3$). (b) Mesh with $N = 4$. (c) Mesh with $N = 8$. In (b) and (c), the solid and dotted lines denote quadrilateral and triangular element meshes, respectively.

We test this bending-dominated shell problem for two different thickness to length (radius) ratios: $t/L = 4/1000$ and $4/10,000$ ($L = R$). The corresponding load magnitudes are $P = 2.0$ and 2.0×10^{-3} , respectively. The reference displacement of $u_{ref} = 0.0924$ at point A [28] is used. In this problem, both membrane locking and shear locking can occur.

Table 16
Normalized displacement at the point of load application (point A) for the hemispherical shell with cut-out problem with the distorted mesh in Fig. 17(c).

t/R	N	3-node element MITC3+	4-node elements		
			S4	MITC4	MITC4+
4/1000	4	1.033	0.1668	0.0397	0.8659
	8	1.016	0.5715	0.1556	0.9736
	16	1.009	0.9304	0.5815	0.9958
	32	1.006	0.9973	0.9437	1.003
	64	1.006	1.005	1.001	1.005
4/10,000	4	1.030	0.0031	0.0005	0.5502
	8	1.006	0.0251	0.0040	0.9048
	16	0.9949	0.1586	0.0280	0.9736
	32	0.9888	0.6412	0.1774	0.9807
	64	0.9858	0.9457	0.6936	0.9831

Reference solution: 9.3000×10^{-2}

Fig. 20 and **Table 17** show the convergence of the normalized displacement (u_A/u_{ref}) at point A. The MITC3+ and MITC4+ shell elements present a good performance compared to the other shell elements considered in this study.

3.9. Hyperbolic paraboloid shell problem

We consider the hyperbolic paraboloid shell problem shown in **Fig. 21**. The mid-surface of the shell structure is given by

$$z = y^2 - x^2; \quad x, y \in [-1/2, 1/2]. \quad (3)$$

This is a doubly-curved shell with negative Gaussian curvature, which makes the problem difficult to solve.

The shell structure is clamped at one edge and subjected to its self-weight. Due to symmetry, only one-half of the structure corresponding to the shaded region ABCD in **Fig. 21(a)** is modeled, with the following boundary conditions: $u = \beta = 0$ ($u = \theta_y = \theta_z = 0$) along CD, and $u = v = w = \alpha = \beta = 0$ ($u = v = w = \theta_x = \theta_y = \theta_z = 0$) along AD. The solutions are obtained using $N \times 2N$ element meshes with $N = 4, 8, 16, 32$, and 64 . The regular and distorted mesh patterns in **Fig. 9(b)** and (c) are used as shown in **Fig. 21(b)** and (c), respectively.

In this bending-dominated shell problem, we test two different thickness to length ratios: $t/L = 1/1000$ and $1/10,000$. The

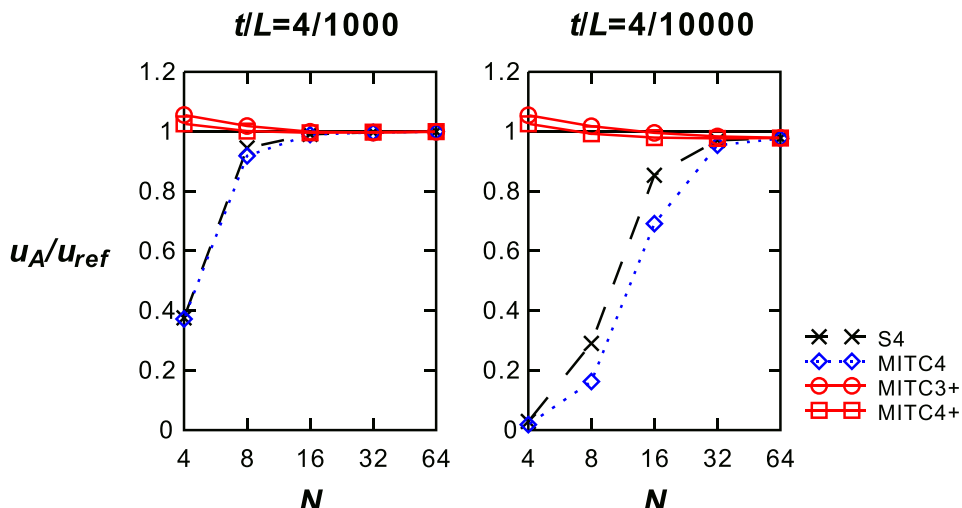


Fig. 20. Convergence of normalized displacement at point A for the full-hemisphere shell problem.

Table 17

Normalized displacement at the point of load application (point A) for the full hemisphere shell problem.

t/R	N	3-node elements		4-node elements				
		MITC3+	TRIC3	S4	MITC4	MITC4+	SIMO4	DKQ4
4/1000	4	1.056	1.022	0.3761	0.3722	1.026	0.651	0.753
	8	1.019	1.013	0.9450	0.9186	1.002	0.968	0.985
	16	0.9994	1.000	0.9908	0.9899	0.9960	0.993	0.998
	32	0.9965	–	0.9977	0.9971	0.9982	–	–
	64	0.9992	–	1.000	0.9996	0.9999	–	–
4/10000	4	1.055	–	0.0289	0.0182	1.026	–	–
	8	1.018	–	0.2904	0.1625	0.9926	–	–
	16	0.9956	–	0.8536	0.6915	0.9798	–	–
	32	0.9837	–	0.9705	0.9541	0.9771	–	–
	64	0.9791	–	0.9781	0.9766	0.9784	–	–

Reference solution: 9.2400×10^{-2}

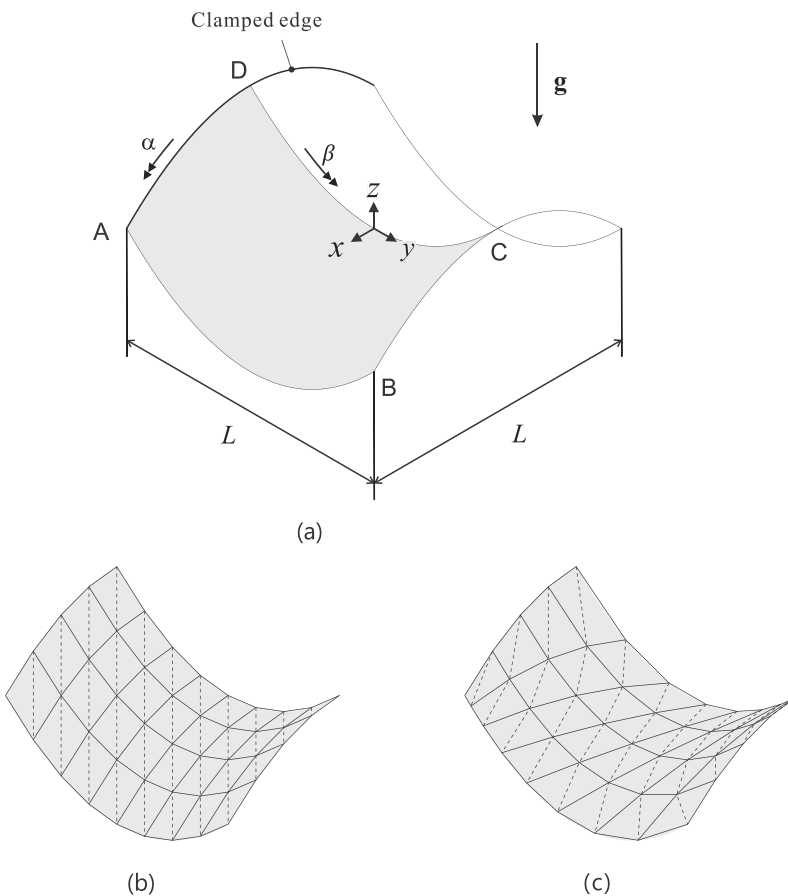


Fig. 21. Hyperbolic paraboloid shell problem. (a) Problem description ($L = 1.0$, thickness $t = 0.001$ and 0.0001 , density $\rho = 360$ and 360×10^{-2} , acceleration of gravity \mathbf{g} with magnitude 1.0, $E = 2.0 \times 10^{11}$ and $v = 0.3$). (b) The regular mesh with $N = 4$. (c) The distorted mesh in Fig. 9(c) used here ($N = 4$). In (b) and (c), the solid and dotted lines denote quadrilateral and triangular element meshes, respectively.

corresponding load magnitudes are scaled by using the densities $\rho = 360$ and 360×10^{-2} , respectively. We use the reference displacements at the center of the free edge, point C, established using a 72×144 mesh of MITC9 shell elements: $w_{ref} = 2.8780 \times 10^{-4}$ and $w_{ref} = 2.3856 \times 10^{-4}$ for $t/L = 1/1000$ and $1/10,000$, respectively. The two reference displacements are different due to the presence of the membrane strain energy [6].

Fig. 22 and Tables 18–19 show the convergence of the normalized displacement (w_C/w_{ref}) at point C. Once again, the MITC3+ and

MITC4+ shell elements converge well while the performance of the other shell elements severely deteriorates when the mesh is distorted.

4. Concluding remarks

We have tested the performance of the new MITC shell elements (the MITC3+ and MITC4+ elements) through a set of widely-used benchmark problems. The problems considered are

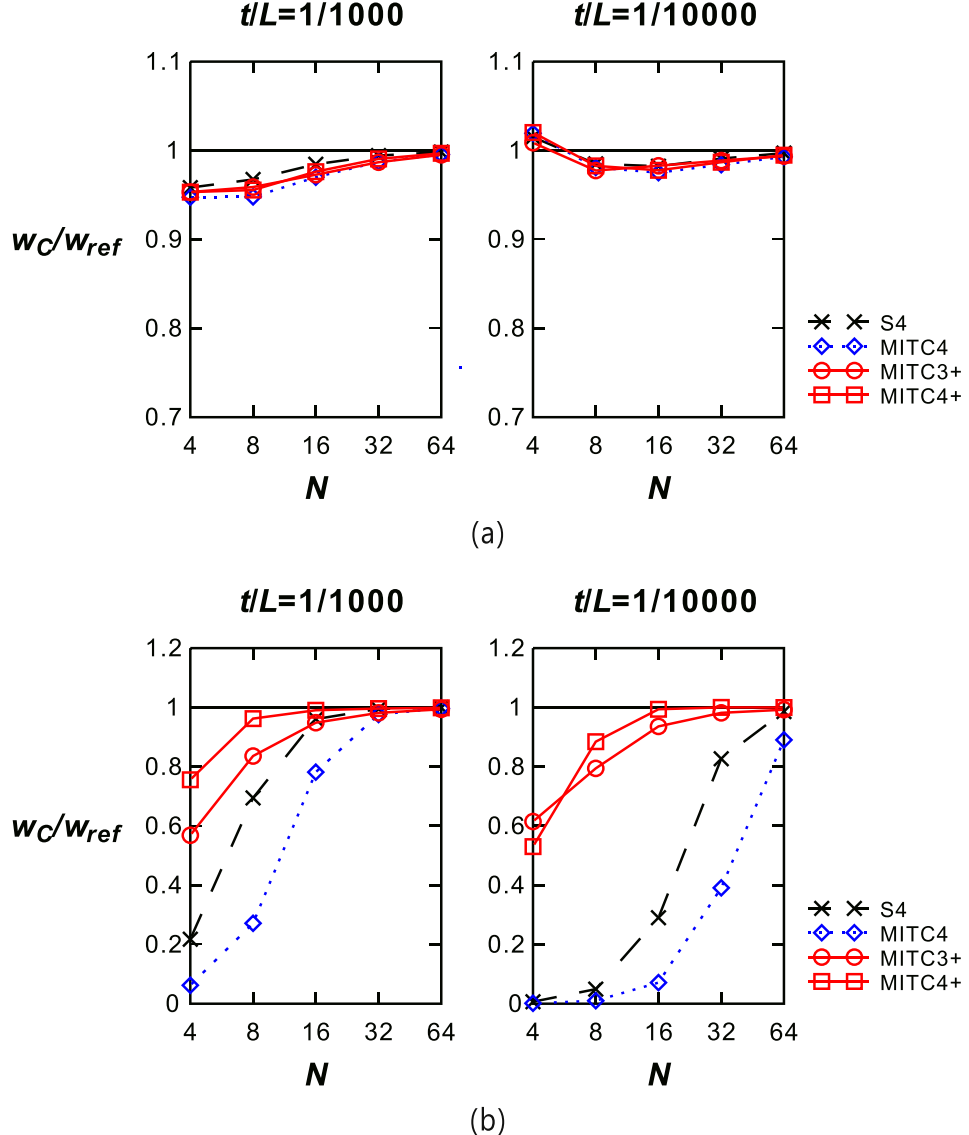


Fig. 22. Convergence of normalized displacement at point C for the hyperbolic paraboloid shell problem with the (a) regular and (b) distorted meshes.

Table 18

Normalized displacement at the center of free edge (point C) for the hyperbolic paraboloid shell problem with the regular mesh in Fig. 21(b).

t/L	N	3-node element		4-node elements		
		MITC3+	S4	MITC4	MITC4+	
1/1000	4	0.9533	0.9582	0.9475	0.9532	
	8	0.9589	0.9674	0.9479	0.9555	
	16	0.9728	0.9846	0.9699	0.9762	
	32	0.9868	0.9943	0.9873	0.9906	
	64	0.9951	0.9983	0.9956	0.9969	
	Reference solution: 2.8780×10^{-4}					
1/10000	4	1.009	1.015	1.019	1.020	
	8	0.9774	0.9850	0.9809	0.9827	
	16	0.9828	0.9823	0.9750	0.9777	
	32	0.9886	0.9910	0.9840	0.9868	
	64	0.9937	0.9971	0.9929	0.9947	
	Reference solution: 2.3856×10^{-4}					

Table 19

Normalized displacement at the center of the free edge (point C) for the hyperbolic paraboloid shell problem with the distorted mesh in Fig. 21(c).

t/L	N	3-node element		4-node elements		
		MITC3+	S4	MITC4	MITC4+	
1/1000	4	0.5685	0.2176	0.0622	0.7559	
	8	0.8359	0.6945	0.2714	0.9622	
	16	0.9483	0.9607	0.7814	0.9904	
	32	0.9816	0.9948	0.9760	0.9962	
	64	0.9936	0.9990	0.9969	0.9988	
	Reference solution: 2.8780×10^{-4}					
1/10000	4	0.6149	0.0007	0.0001	0.5302	
	8	0.7943	0.0492	0.0010	0.8843	
	16	0.9358	0.2902	0.0711	0.9936	
	32	0.9816	0.8267	0.3909	1.000	
	64	0.9922	0.9859	0.8903	0.9995	
	Reference solution: 2.3856×10^{-4}					

mostly bending dominated problems including various geometries and loading conditions: from plate to doubly curved shell problems of moderately thick to thin structures, and distributed loading and concentrated load conditions. Like in the papers giving solutions to the widely-used benchmark tests, we focused on displacements at some points. Through the convergence studies including comparisons with other elements, the performance of the MITC3+ and MITC4+ shell elements is shown to be consistently good even when distorted meshes are used. However, we did not consider the analysis of thick and composite structures in which shear effects can be important.

Once more we have demonstrated that while a shell element may perform very well in regular meshes, its performance may severely deteriorate in distorted meshes [3–5]. Therefore, the performance of shell elements should be thoroughly tested in both regular and properly selected distorted meshes. The numerical data provided in this study should be beneficial for the evaluation of many plate and shell finite elements.

Acknowledgments

This research was supported by a grant (MPSS-CG-2015-01) through the Disaster and Safety Management Institute funded by Ministry of Public Safety and Security of Korean government, and the Climate Change Research Hub of KAIST (No. N11170061).

References

- [1] Chapelle D, Bathe KJ. Fundamental considerations for the finite element analysis of shell structures. *Comput Struct* 1998;66(1):19–36, 711–2.
- [2] Chapelle D, Bathe KJ. The finite element analysis of shells – fundamentals. 2nd ed. Berlin: Springer; 2011.
- [3] Lee Y, Lee PS, Bathe KJ. The MITC3+ shell element and its performance. *Comput Struct* 2014;138:12–23.
- [4] Ko Y, Lee PS, Bathe KJ. A new MITC4+ shell element. *Comput Struct* 2017;182:404–18.
- [5] Ko Y, Lee PS, Bathe KJ. A new 4-node MITC element for analysis of two-dimensional solids and its application in shell analyses. *Comput Struct* 2017;192:34–49.
- [6] Lee PS, Bathe KJ. On the asymptotic behavior of shell structures and the evaluation in finite element solutions. *Comput Struct* 2002;80(3):235–55.
- [7] Bathe KJ. The inf-sup condition and its evaluation for mixed finite element methods. *Comput Struct* 2001;79(2):243–52.
- [8] Bathe KJ, Iosilevich A, Chapelle D. An inf-sup test for shell finite elements. *Comput Struct* 2000;75(5):439–56.
- [9] Bathe KJ. Finite element procedures. Prentice Hall; 1996, 2nd ed. KJ Bathe, Watertown, MA; 2014 and Higher Education Press, China; 2016.
- [10] Dvorkin EN, Bathe KJ. A continuum mechanics based four-node shell element for general nonlinear analysis. *Eng Comput* 1984;1(1):77–88.
- [11] Lee PS, Bathe KJ. Development of MITC isotropic triangular shell finite elements. *Comput Struct* 2004;82(11):945–62.
- [12] Hiller JF, Bathe KJ. Measuring convergence of mixed finite element discretizations: an application to shell structures. *Comput Struct* 2003;81(8):639–54.
- [13] MacNeal RH, Harder RL. A proposed standard set of problems to test finite element accuracy. *Finit Elec Anal Des* 1985;1(1):3–20.
- [14] ABAQUS 6.12 Theory manual. Dassault Systèmes Simulia Corp., Providence, Rhode Island; 2012.
- [15] Batoz JL, Bathe KJ, Ho LW. A study of three-node triangular plate bending elements. *Inter J Num Meth Eng* 1980;15:1771–812.
- [16] Bathe KJ, Ho LW. A simple and effective element for analysis of general shell structures. *Comput Struct* 1981;13(5–6):673–81.
- [17] Batoz JL, Zheng CL, Hammadi F. Formulation and evaluation of new triangular, quadrilateral, pentagonal and hexagonal discrete Kirchhoff plate/shell elements. *Inter J Num Meth Eng* 2001;52(5–6):615–30.
- [18] Batoz JL, Katili I. On a simple triangular Reissner/Mindlin plate element based on incompatible modes and discrete constraints. *Inter J Num Meth Eng* 1992;35(8):1603–32.
- [19] Katili I. A new discrete Kirchhoff-Mindlin element based on Mindlin-Reissner plate theory and assumed shear strain fields—part II: an extended DKQ element for thick-plate bending analysis. *Inter J Num Meth Eng* 1993;36(11):1885–908.
- [20] Simo JC, Fox DD, Rifai MS. On a stress resultant geometrically exact shell model. Part II: The linear theory; computational aspects. *Comput Meth Appl Mech Eng* 1989;73(1):53–92.
- [21] Ibrahimović A, Frey F. Stress resultant geometrically non-linear shell theory with drilling rotations. Part III: Linearized kinematics.. *Inter J Num Meth Eng* 1994;37(21):3659–83.
- [22] Bletzinger KU, Bischoff M, Ramm E. A unified approach for shear-locking-free triangular and rectangular shell finite elements. *Comput Struct* 2000;75(3):321–34.
- [23] Lee PS, Noh HC, Bathe KJ. Insight into 3-node triangular shell finite elements: the effects of element isotropy and mesh patterns. *Comput Struct* 2007;85(7):404–18.
- [24] Koschnick F, Bischoff M, Camprubí N, Bletzinger KU. The discrete strain gap method and membrane locking. *Comput Meth Appl Mech Eng* 2005;194(21):2444–63.
- [25] Argyris J, Tenek L. An efficient and locking-free flat anisotropic plate and shell triangular element. *Comput Meth Appl Mech Eng* 1994;118(1):63–119.
- [26] Argyris JH, Papadakakis M, Apostolopoulou C, Koutsourelakis S. The TRIC shell element: theoretical and numerical investigation. *Comput Meth Appl Mech Eng* 2000;182(1):217–45.
- [27] Timoshenko S, Woinowsky-Krieger S. Theory of plates and shells. 2nd ed. New York: McGraw-Hill; 1959.
- [28] Belytschko T, Stolarski H, Liu WK, Carpenter N, Ong JS. Stress projection for membrane and shear locking in shell finite elements. *Comput Meth Appl Mech Eng* 1985;51(1):221–58.
- [29] Belytschko T, Wong BL, Stolarski H. Assumed strain stabilization procedure for the 9-node Lagrange shell element. *Inter J Num Meth Eng* 1989;28(2):385–414.
- [30] Knight NF. Raasch challenge for shell elements. *AIAA J* 1997;35(2):375–81.